

RESEARCH

Open Access



Bioelectronic osteosynthesis plate to monitor the fracture bone healing using electric capacitive variations

Diogo G. Pires^{1*}, Nuno M. Silva², A. Completo^{1,3} and Marco P. Soares dos Santos^{1,3*}

Abstract

Background Bone fractures represent a global public health issue. Over the past few decades, a sustained increase in the number of incidents and prevalent cases have been reported, as well as in the years lived with disability. Current monitoring techniques predominantly rely on imaging methods, which can result in subjective assessments, and expose patients to unnecessary cumulative doses of radiation. Besides, they are costly and incapable of providing continuous daily detection of fracture healing stages. Technological advances are still required to design fixation systems with the ability to minimize the risk of delayed healing and nonunion conditions for timely medical intervention, such that preventive procedures can be provided. This work proposes.

Methods An innovative bioelectronic osteosynthesis plate, minimally customized from a fixation device used in clinical practice, was developed to monitor the bone-implant interface to effectively detect the progression of bone fractures stages. Our technology includes a network-architected capacitive interdigitated system, a Bluetooth module, an analog-to-digital converter, a multiplexer, a microcontroller, and a miniaturized battery.

Results Both experimental tests with biological tissues and numerical simulations show strong evidence that this bioelectronic implant is able: (i) to detect the four distinct bone healing stages, with capacitance decreases throughout the healing process; and (ii) to monitor the callus formation across multiple target regions.

Conclusions This work provides a significant contribution to the design of bioelectronic implant technologies for highly personalized sensing of biointerfaces. Our bioelectronic fixation implant supports faster fracture healing, mainly for delayed healing and non-union conditions.

Keywords Instrumented implant, Bone fracture healing, Bioelectronic implants, Capacitive sensing, Healing monitoring

*Correspondence:

Diogo G. Pires

diogogp24@ua.pt

Marco P. Soares dos Santos

marco.santos@ua.pt

¹Department of Mechanical Engineering, Centre for Mechanical Technology & Automation (TEMA), University of Aveiro, Aveiro 3810-193, Portugal

²Department of Engineering, University of Trás-os-Montes e Alto Douro, Vila Real 5000-801, Portugal

³Intelligent Systems Associate Laboratory (LASI), Guimarães 4800-058, Portugal



© The Author(s) 2025. **Open Access** This article is licensed under a Creative Commons Attribution-NonCommercial-NoDerivatives 4.0 International License, which permits any non-commercial use, sharing, distribution and reproduction in any medium or format, as long as you give appropriate credit to the original author(s) and the source, provide a link to the Creative Commons licence, and indicate if you modified the licensed material. You do not have permission under this licence to share adapted material derived from this article or parts of it. The images or other third party material in this article are included in the article's Creative Commons licence, unless indicated otherwise in a credit line to the material. If material is not included in the article's Creative Commons licence and your intended use is not permitted by statutory regulation or exceeds the permitted use, you will need to obtain permission directly from the copyright holder. To view a copy of this licence, visit <http://creativecommons.org/licenses/by-nc-nd/4.0/>.

Introduction

Bone fractures are one of the most common injuries, being associated with high treatment costs, reduced social productivity, and increased disability. The total number of cases has grown significantly over the last decades. More than 178 million fractures are reported worldwide per year [1], and yet the non-union rates can surpass 10%, particularly in the healing of long bones [1, 2]. Significant increases in prevalence among people in active age groups have been also reported, emphasizing the vital role of efficient fracture management in mitigating disability, productivity loss, and reduced quality of life [1]. Currently, monitoring methods used in medical practice only rely on image analysis [3, 4]. The most used technique is radiography; however, delayed healing or non-union scenarios, the most common early complications after the implant insertion, are hardly detected on radiographic images, mainly due to scarcity of mineralized tissue [5]. Besides, this method has relevant disadvantages, mainly its high subjectivity, a non-negligible health risk for patients due to accumulated radiation doses, high cost and inability to provide daily monitoring of fracture healing stages [3, 4]. There is a need for new technologies capable of quantitatively monitoring bone fractures to effectively surpass these limitations. A highly promising approach to monitor bone fracture healing is the use of instrumented devices exploring changing biophysical properties of fractured bones. Mechanical vibration [6], electrical impedance [7, 8] and electromagnetic radiation [9] were the methods already proposed for external fixators. Regarding osteosynthesis plates, which are commonly used for stabilizing long bone fractures (particularly those of the distal tibia and femur), detection methodologies include the use of mechanical vibration [10], electric impedance [7, 11, 12], electromagnetic radiation [13], electric charge [14] and mechanical displacement [15]. Intramedullary nails were also designed embedding sensing systems to track the biomechanical biointerface between fractured sites, even though they were limited to mechanical vibration [16] and electromagnetic radiation [17]. Significant improvements related to bone-implant callus monitoring were obtained in comparison to conventional imaging methods, including higher resolution and sensitivity. However, these developed technologies still have severe limitations: (i) they do not allow effective monitoring of multiple regions for spatiotemporal detection; (ii) extracorporeal excitations are required; (iii) they can only detect early stages of bone/implant disorders with low accuracy (e.g. delayed fracture healing); and (iv) they can require significant changes in the implant design, as well as in the surgical procedure. Another strategy to monitor fracture healing is by analyzing some biological markers. Recent studies have revealed that stress-induced hyperglycemia

parameters, such as fasting blood glucose, postprandial glucose, and HbA1c, may be used as predictive markers for delayed healing after tibial fracture surgery [18]. Additionally, LINC00339, a long non-coding RNA, has been shown to significantly affect fracture healing by regulating osteoblast function, and may also be used as a diagnostic marker in assessing delayed fracture healing [19]. Furthermore, miR-1271-5p is also an important marker for delayed healing in fractured bones, particularly in the context of pilon fractures, and may offer new insights for treatment strategies [20]. Recent research also suggests that the CASC11 and miR-150-3p are involved in osteoblast differentiation, working together as osteogenic marker genes, allowing for an early detection of delayed fracture healings [21].

By engineering bioelectronic bone implants, futuristic breakthroughs in orthopaedic implant technology can be achieved. These are advanced implants that hold potential to integrate electronic systems supporting various functions, including monitoring of biointerfaces (included between fixations implants and fractured regions) and communication between the implant and medical specialists, all of them supported by self-powering systems [22–26]. Recent advancements provide strong evidence that co-surface capacitive patterns can be integrated into bioelectronic implants for ultrasensitive detection ability [24, 27]. They can ensure sub-femto-farad resolution, exceptional scalability, and the capability to personalize the monitoring of complex biointerfaces, including those involving bioactive materials [24, 27, 28].

In this study, we propose a bioelectronic osteosynthesis plate, instrumented with an ultrasensitive capacitive sensing technology to effectively monitor the healing process in multiple target regions along fractured regions (Fig. 1). It was also engineered including a communication module for remote data transfer, a processing unit and a battery system to avoid external inductive powering. An implant prototype was implemented using a commercialized fixation device, in which minimal customization changes were performed, such that surgical procedure changes would not be required. An interdisciplinary study is here presented to provide: (i) computational models, such that capacitive variations in the four different stages of fracture bone healing (hematoma, soft callus, hard callus and remodeling) can be predicted. (ii) A prototype of a bioelectronic osteosynthesis plate, including all electronics for sensing, processing, communicating and electric powering. Design modifications were performed to ensure similar mechanical proprieties as the original one. (iii) Experimental validation using biological tissues of the computational models and the sensing effectiveness of this sensing implant. This bioelectronic fixation implant is focused on a new concept that holds potential to allow faster fracture healing

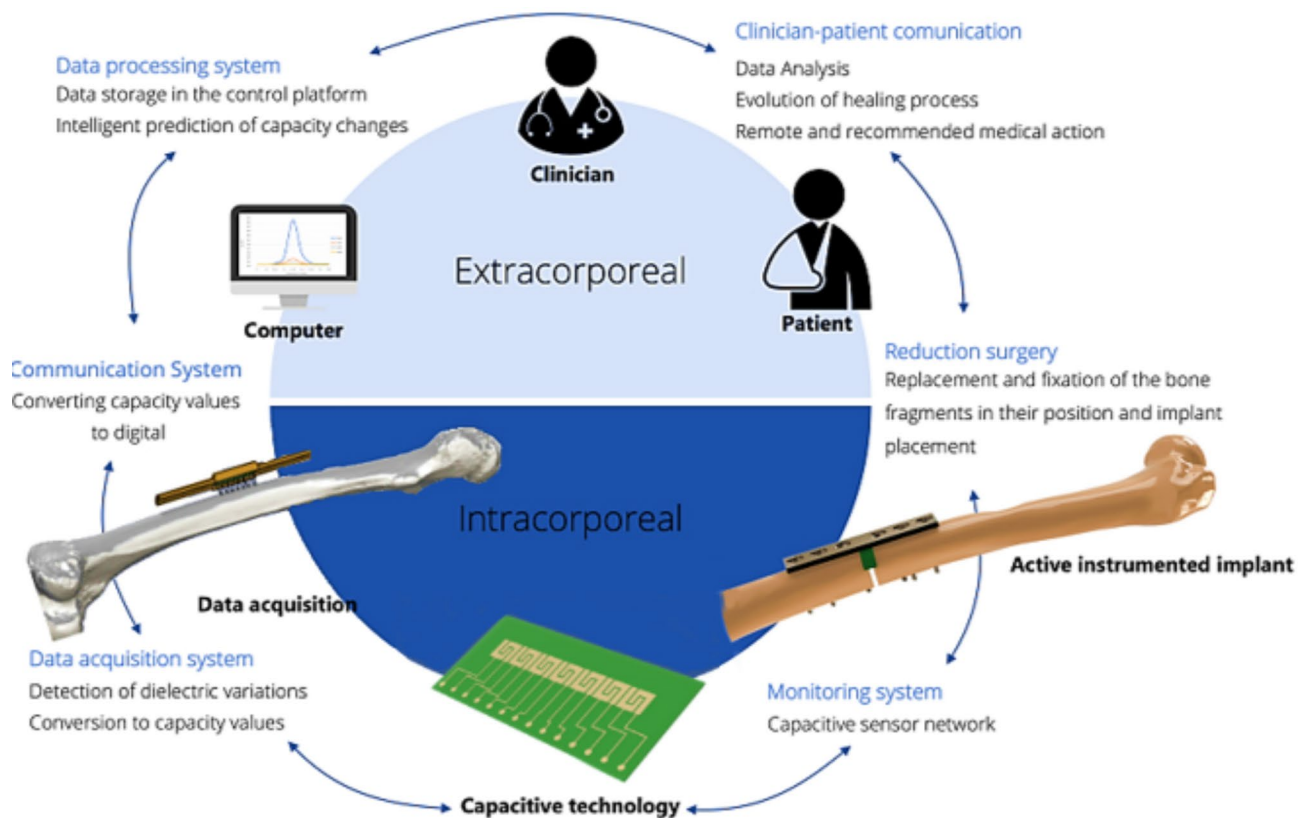


Fig. 1 Schematic overview of the proposed bioelectronic multifunctional fixation system

(using data related to the healing progression), mainly for delayed healing and non-union conditions.

Materials and methods

The new bioelectronic implant concept

Sensing system and working principle

A miniaturized biomedical circuit was implemented comprising two PCB boards with $34 \times 15 \text{ mm}^2$: (i) a modular structure for capacitance measurement, data processing, electric power management and communication (Fig. 2a); and (ii) a network of 7 capacitive interdigitated sensors (Fig. 2b). The spatial resolution of monitoring system correspond to the related electrode dimensions ($2.5 \times 2.75 \text{ mm}^2$), along a total detection area of $25.25 \times 2.5 \text{ mm}^2$, which is obtained by: (1) the electrode dimensions of $2.5 \times 2.75 \text{ mm}^2$ with 0.5 mm spacing between the plates within each interdigitated electrode pair, allowing for high sensitivity to capacitance variations in that specific region; and (2) the 1 mm spacing between adjacent electrodes, defining the ability to detect multiple variations across a larger region. Even though capacitive variations cannot be measured at regions between electrodes, our monitoring system is capable of distinguishing variations at both the intra- and inter-electrode levels, providing a comprehensive spatial detection capability across the monitored area.

The detection principle of our capacitive sensing system relies on variations in electric capacitive reactance (X_C), which occur as the dielectric properties of bone tissues evolve during the fracture healing process. The capacitive reactance can be expressed by the following equation:

$$X_C = -\frac{1}{2\pi fC}, \quad (1)$$

where f represents the frequency of the electric field, and C is the capacitance of the dielectric medium. The dielectric properties of biological tissues change throughout the stages of callus formation (from blood hematoma to fully restored bone). These changes result in variations in capacitance δC , and, for a specific frequency f , the capacitive reactance X_C changes accordingly [29]. Indeed, the relative permittivity ϵ_r (or dielectric constant) of the fractured bone is related to the applied electric displacement field D and the electric field E , as follows:

$$D = \epsilon E, \quad (2)$$

$$\epsilon_r = \frac{\epsilon}{\epsilon_0}, \quad (3)$$

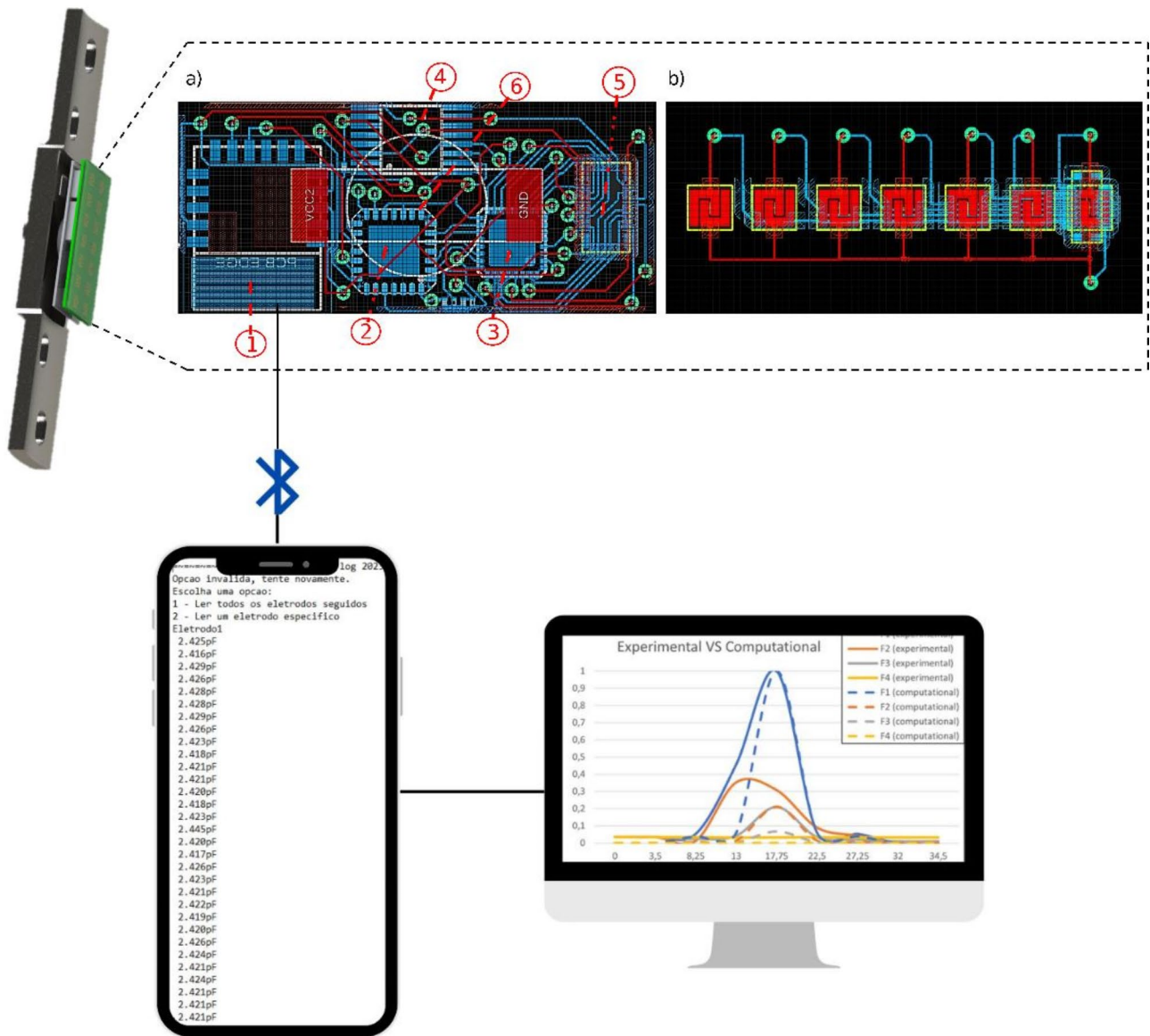


Fig. 2 Overall monitoring system including the bioelectronic osteosynthesis plate, and computational analysis using smartphone and computer systems. Illustration of PCB boards: **a)** PCB modular structure comprising: 1: RN4871 Bluetooth Module; 2: PIC16LF1847; 3: ADG1606 Multiplexer; 4: AD7745 Analog-to-Digital Converter; 5: 16-Pin Connector; 6: CR1216 Miniaturized Battery; **b)** PCB matrix-structured network of interdigitated and striped capacitive systems

where ϵ_0 is the vacuum permittivity, and ϵ is the frequency-dependent permittivity. As the capacitance C of the fractured region is defined as the ability of the fractured bone macroenvironment to store electric charge Q per unit of voltage V , and using the Gauss’s law, then

$$C = \frac{dQ}{dV} \tag{4}$$

and

$$E = \hat{r} \frac{Q}{4\pi r^2 \epsilon} , \tag{5}$$

where r is the distance from the charges flowing through the fractured bone tissues, and \hat{r} is a unit vector pointing away from the charges. These analytical formulations express how the electric field strength applied to fractured bones during capacitive sensing is strongly influenced by the sensor-bone distance, as well as the permittivity-dependent callus evolution. During the healing progression, changes in the bone structure occur. Initially, the hematoma stage features a blood clot, which exhibits a higher conductivity compared with the ones exhibited by both cartilaginous structures and cortical and trabecular bone structures, resulting in lower electric field strength. As healing progresses, and soft and

hard callus develop, the bone's conductivity decreases, resulting in increased electric field strengths. Finally, during the remodeling stage, mature bone tissue with improved organization and conductivity leads to the highest electric field strength. Using our computational models (described in Sect. 2.2), we found that fracture-sensor interfaces exhibit different maximum electric field strengths delivered to the bone throughout bone healing: in the intact-fractured transition from the fractured region to the cortical bone, 0.053 V/mm was obtained for the hematoma stage, as well as 0.084 V/mm for the soft callus stage, 0.126 V/mm for the hard callus stage, and 0.183 V/mm for the remodeling stage. These magnitudes may change in clinical practice due to various causes, mainly the patient idiosyncrasies, fracture type, fracture severity, sensor-bone distance (due to the mechanical fixation after surgical procedures), which requires a normalization of the capacitive variations (described in Sect. 4). In this study, capacitance measurements were performed using both AC excitation and measurement, as capacitive reactance is a frequency-dependent quantity (Eq. 1), and the electric field distributions along the fractured bone structure are related to the alternating displacement currents flowing through it (Eq. 2).

Biomedical electric circuit

A Bluetooth Low Energy (BLE)-based communication module (RN4871, Microchip Technology) was used to enable remote control and data transfer related to the sensing operation. The PIC microcontroller (PIC16LF1847, Microchip) was used such that low-power consumption requirements (3.3 V @ 32 μ A) can be fulfilled. Besides it supports both I2C and Serial Peripheral Interface (SPI) communication protocols, the PIC16LF1847 also includes an ultra-low power sleep mode (2 V @ 13 μ A), for feasible engineering of activation circuits in battery systems for biomedical implantable systems [30]. Data-acquisition was established by a high-resolution 24-bit Capacitance-to-Digital Converter (CDC) (AD7745, Analog Devices). This electric component offers exceptional resolution (4 aF), precision (4 fF), full-scale capacitance range (± 4 pF), and power consumption (3.3 V @ 0.7 mA). A Li-ion battery, CR1216 with 25 mAh was used, as osteosynthesis plates are typically implanted for brief periods of time (less than one year) [2]. One 8-channel multiplexer (ADG1606, Analog Devices) was incorporated to select which capacitor must be monitored, via the CDC chip (AD7745; sensing operation), both to prevent parasitic capacitances and allow electrode-microcontroller communication. Figure 2 presents the main electric connections. This AD7745 module collects data from the biointerface between tissues and the fractured bone regions, and performs data transmission to the PIC microcontroller. 200 measurements per

electrode were delivered via Bluetooth to a smartphone (A2221, Apple) using the SmartData application (v. 1.1, Microchip Technology Inc.). All data was uploaded to a .csv file and processed on a computer for statistical analysis.

Customization of osteosynthesis plate

A commercialized locking osteosynthesis plate of 18 holes (158.118, Narang Medical Limited) was the physical model used to carry out slight customizations related to the incorporation of the biomedical circuit. Such modifications were performed in the central region over $15.5 \times 34.5 \times 6$ mm³ (Fig. 3a), such that similar mechanical properties as the original plate can ensure structural integrity. The bulk part of the prototype was manufactured using a 3-axis CNC MIKRON machine (GF Machining Solutions), and the G-code used for the machining process was generated using SolidWorks CAM.

Electrodes were positioned in the nearest region interfacing the fractured bone (Fig. 3b), according to a Euclidean distance dependent of the healing phase, namely ≈ 0 mm for the inflammatory phase, ≈ 0.67 mm for the repair phase with soft callus formation, ≈ 1.33 mm for the repair phase with hard callus formation, and, finally, ≈ 2 mm the remodeling phase. An opening, corresponding to an area of (5×3.5 mm²) of biocompatible polymer coating, was designed in the upper surface (on the side opposite to the electrodes) to allow reliable data communication between the BLE module and the smartphone. This opening is positioned directly above the soldered BLE module, precisely at the location where the ceramic chip antenna was integrated to ensure an unattenuated path for signal transmission. Additionally, the used BLE module incorporates a dedicated metal-free zone around the antenna on its PCB. Together, these design considerations mitigate interferences from the metallic encapsulation, ensuring effective BLE communication with extracorporeal systems without requiring further adaptations. While the metallic environment may slightly reduce the communication range, the combined features are enough to keep reliable data transmission. The stainless steel AISI 316 L was used as the bulk material for the bioelectronic fixation system, similarly to the commercialized one [31, 32].

2.1.4. Power consumption

The current consumption was measured at the battery output during a capacitance measure of a pair of interdigitated electrodes and using the Ohm's law. The power consumption of the device was assessed by using Lebesgue integral to the current consumption over the duration of a monitoring session. As capacitance monitoring requires 5 s per pair of interdigitated electrodes, only

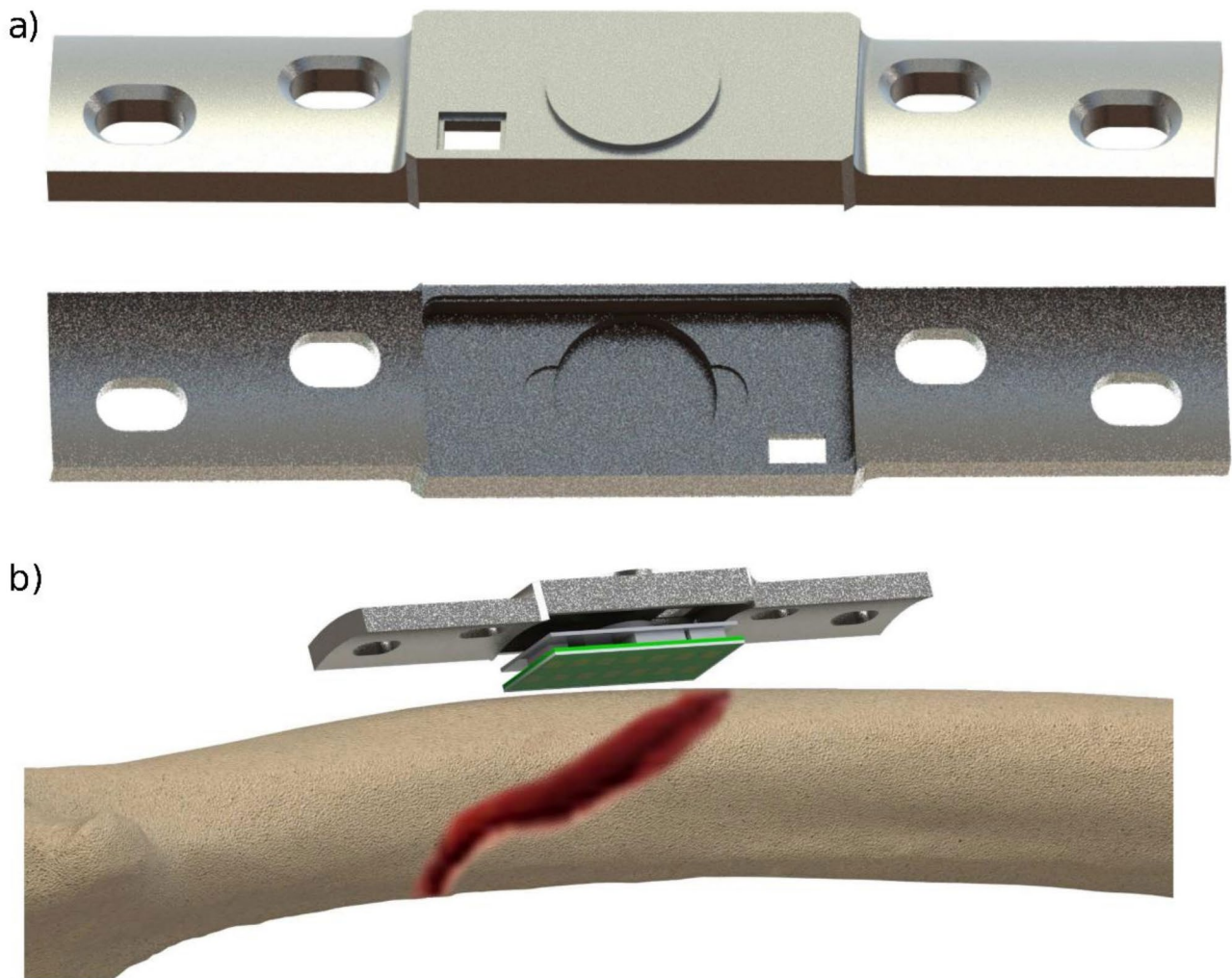


Fig. 3 a) Model of the new modified locking plate; b) Concept of the new capacitive instrumented implant placed over a fractured bone

35 s is required for the reading operation, which results in 2.9562 mAs of total current consumption (28.8 μ Ah). Based on this consumption, our bioelectronic device can support around 868 monitoring sessions on a single battery charge, which allows >2 years of daily monitoring. Even though a higher number of reading operations is expected during the six months post-surgery, particularly in complex cases such as nonunion, where a closer follow-up is crucial, the scheduling of the monitoring sessions must ultimately be defined by clinicians considering the patient's clinical needs (personalized medicine) and battery longevity management (technological limitations).

Computational models

Computational modelling was carried out using SolidWorks (v.2023, Dassult Systemes), to geometrically model all elements related to the bone fracture healing elements. COMSOL Multiphysics (v.6.0, COMSOL) was used to develop the finite element models and simulate

the electric capacitances related to each bone healing stage. Four healing stages were modelled: (i) the inflammatory phase, modelled as blood; (ii) the repair phase, with soft callus formation, modelled as a cartilage structure; (iii) the repair phase, with hard callus formation, modelled as a cancellous structure; and (iv) the remodeling phase, consisting in intact bone. Both cortical and trabecular bones were modelled as simplified cylindrical structures (Fig. 4a). The capacitive sensing system, comprising seven interdigitated capacitors, was positioned 2 mm above the outer bone surface, according to a parallel alignment related to the cylinder surfaces, allowing reduced axial stiffness and enabling non-invasive monitoring of interfragmentary biointerface changes (Fig. 4g) [33, 34]. Electrodes with very high electrical conductivity, were embedded on a polycarbonate substrate 0.5 mm thick, and covered with a polystyrene layer of 0.5 mm thick. As polystyrene provides electrical resistivity, the electric field lines will be neither weakened nor distorted; besides, its biocompatibility ensures safe encapsulation

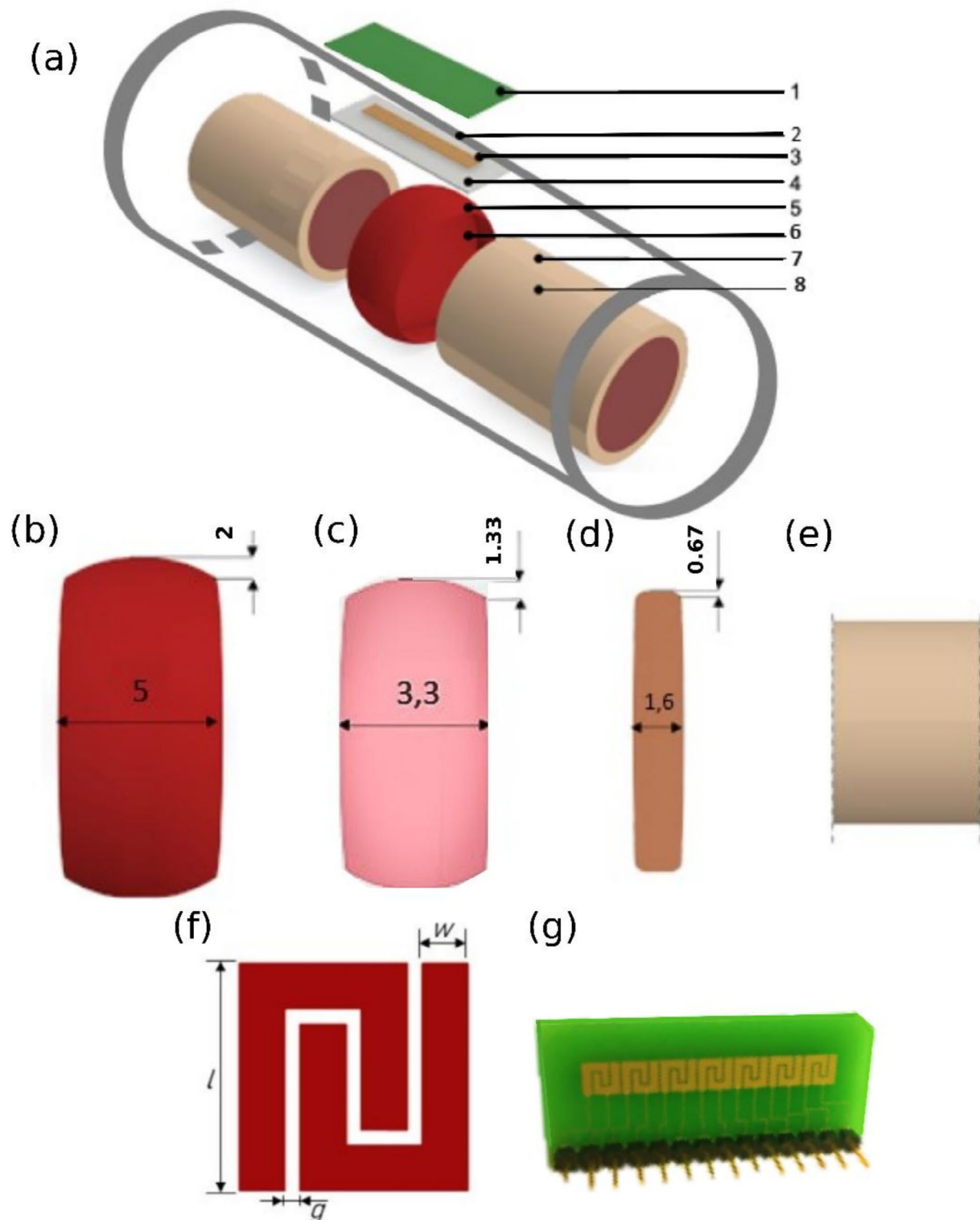


Fig. 4 Domains of computational models to monitor capacitive changes at different healing stages: **(a)** representation of all domains. Representation of the four modeled healing phases: **(b)** inflammatory phase—blood; **(c)** repair phase (soft callus) - cartilage; **(d)** repair phase (hard callus) - trabecular bone; **(e)** remodeling phase - intact bone. Domains: 1: substrate; 2: air; 3: electrodes; 4: polymeric layer; 5: hematoma/bone callus; 6: fracture; 7: cortical bone; 8: cancellous bone. Capacitive architecture: **(f)** interdigitated sensor design ($l = 2.5$ mm; $w = 0.5$; $g = 0.25$ mm); **(g)** PCB board of the co-surface capacitive network

Table 1 Dimensions of bone tissue and capacitive sensor domains

Dimensions of bone tissue domains			
Domain	Length (mm)	Outer diameter (mm)	Inner diameter (mm)
Cortical bone	40.00	30.00	24.56
Trabecular bone	40.00	24.56	---
Fracture	1/0.5/0.25	30.00	---
Blood hematoma	5.0	(max) 32.00	30.00
Soft callus (cartilage)	3.3	(max) 31.33	30.00
Hard callus (trabecular bone)	1.6	(max) 30.67	30.00
Dimensions of capacitive sensor domains			
Domain	Thickness (mm)	Width (mm)	Length (mm)
Electrodes	0.1	2.5	2.75
Substrate	0.5	34.50	15.50
Polymer layer	0.5	34.50	15.50

of the biomedical circuit. All domain dimensions are described in Table 1. Three different fracture thicknesses (1 mm, 0.5 mm and 0.25 mm) were simulated to test the effectiveness of the monitoring system for different fracture-implant biointerfaces.

The AC/DC module (physics interface: 'Electric Current') of COMSOL Multiphysics (v. 6.0, COMSOL) was used to compute the electric capacitance related to each individual interdigitated pair of electrodes. Domains were established as homogeneous and isotropic, and modelled using refined 3D of 2nd linear tetrahedral elements (Delaunay method). A convergence analysis, based on the 2% error criterion, was defined to perform the mesh refinement. Concerning boundaries, a homogeneous Neumann condition was used to the inner ones, and electric isolation for the outer ones. Table 2 defines the electric properties of all domains. Each pair of electrodes were powered by a square wave voltage V (one positively charged, and the other grounded) defined as

$$V = \frac{V_{pp}}{2} + \frac{V_{pp}}{2} \text{sign}(\sin(2\pi ft)), \quad (6)$$

where $V_{pp} = 3 \text{ V}$ is the peak voltage, and $f = 32 \text{ kHz}$ is the excitation frequency. Capacitive changes along the fractured region were calculated by firstly computing individual capacitances C using the admittance Y , as in Eq. 7:

$$C = \frac{\text{Im}(Y)}{2\pi f} \quad (7)$$

Experimental procedure

Mechanical tests

The 3-point bending test was performed to compare the flexural stiffness between a commercialized cobalt-chromium implant and our new bioelectronic implant prototype. This test was conducted using a universal testing machine (AGS-X-10 kN, Shimadzu), with support bases positioned 43 mm apart, a speed rate of 5 mm/min, and a maximum load of 170 N (this range was chosen to avoid exceeding the elastic regime of the commercial plate, such that its permanent deformation can be prevented). As the elastic modulus of cobalt-chromium is 245 GPa, this load was selected to ensure that the material's elastic limit was not exceeded. The new prototype plate was produced in ST37 steel, which has a similar elastic modulus of 235 GPa, such that a similar mechanical performance can be ensured under similar test conditions. Force-displacement analyses were conducted for comparative purposes.

The stiffness of each implant (commercialized vs. prototype) was calculated using the slope of the force-displacement curve, such that we can verify if the prototype stiffness is $\geq 85\%$ of the one provided by the commercialized implant. The target stiffness of 85% was selected as the cross-sectional area of the bioelectronic plate is reduced by the central region for the electronic

Table 2 Electric and magnetic properties of organic and inorganic materials used in computational models for 32 kHz excitation

Domain	Relative Electric Permittivity	Electric Conductivity [S/m]	Relative Magnetic Permeability	Ref.
Substrate	3	6.7×10^{-14}	0.866	[24]
Electrodes	1	6.0×10^7	1	[24]
Polymeric Layer	2.6	6.7×10^{-14}	1	[35]
Cortical Bone	$3.02 \times 10^2 - i1.16 \times 10^4$	0.02	1	[35, 36]
Blood	$6.0 \times 10^1 - i3.93 \times 10^5$	0.7	1	[35, 36]
Trabecular Bone	$7.62 \times 10^2 - i4.67 \times 10^4$	0.07	1	[35, 36]
Cartilage	$4.36 \times 10^1 - i3.26 \times 10^5$	0.58	1	[36]
Air	1	0	1	[24]

components, which makes it less stiff to flexure. This percentage reduction of 15% is reasonable, as it remains within the range of stiffness values found in commercial plates, such as the titanium plates, which present lower flexural stiffness when compared with stainless steel plates.

Capacitive monitoring tests

Concerning monitoring tests, the bioelectronic implant was fixed to a universal testing machine (Shimadzu

AGS-X-10kN; software: Trapezium X) (Fig. 5b), such that the network of capacitive sensors was vertically and centrally positioned 2 mm (accuracy: 1 μ m) above the cortical bone surface, regardless the repair phase (setup valid both for fractured and non-fractured scenarios).

Concerning samples preparation, post-mortem porcine femur samples (aged 8 months) were used to track capacitive changes during the various fracture healing stages. In the inflammatory phase, an oval structure with blood-like dielectric properties was employed to biophysically

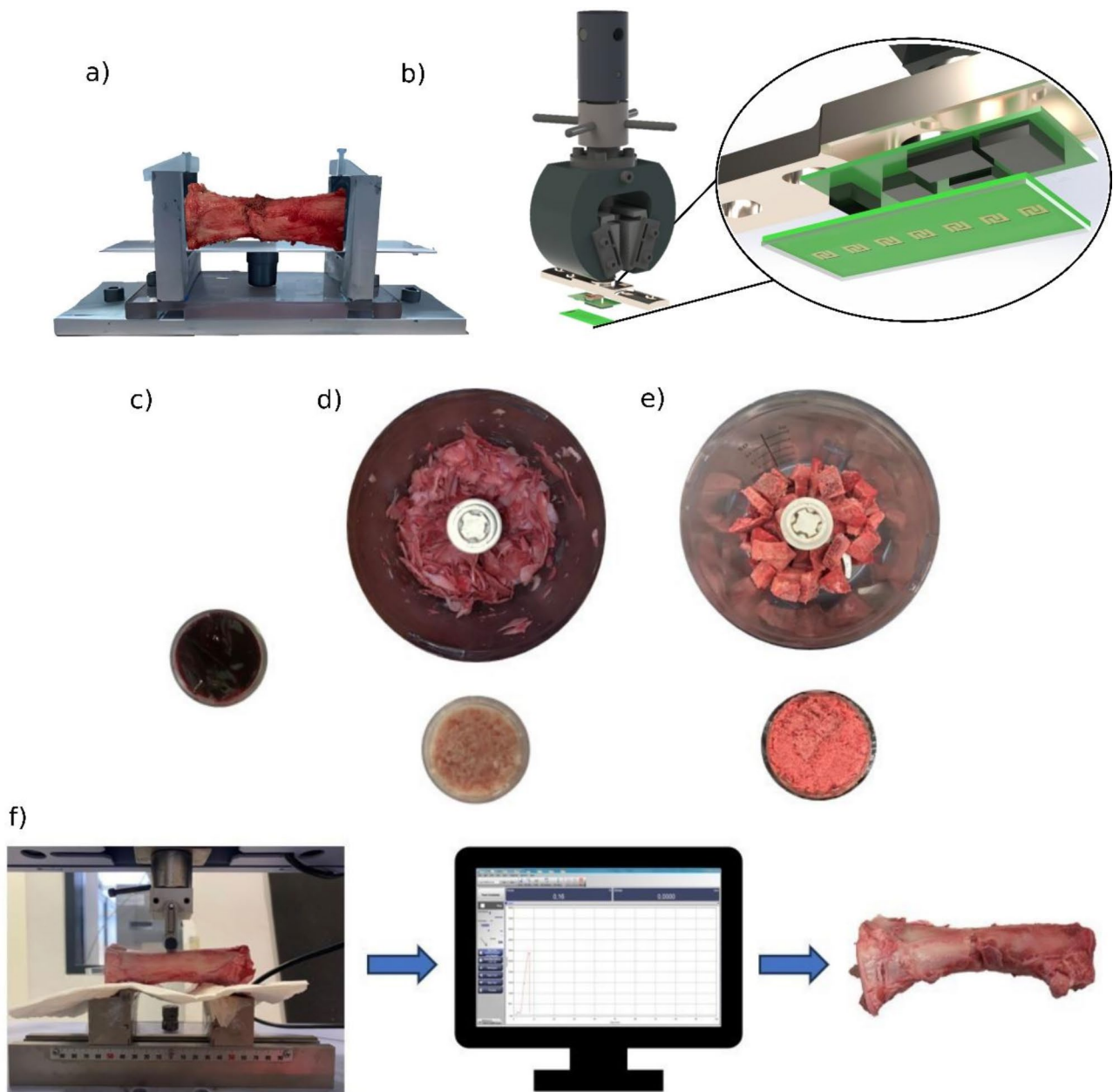


Fig. 5 Experimental apparatus designed for experimental tests with biological tissues: **a)** photo of the structure from the bottom assembly; **b)** detailed view of the components of the top assembly. **c)** Coagulated blood, **d)** cartilage preparation steps and **e)** cancellous bone preparation steps. **f)** View of the fractured bone process. Additional images related to the benchtop setup for different healing stages are available in Supplementary Fig. S1

model the hematoma, which results due to the rupture of blood vessels when bones are fractured. Coagulated blood was used, as this hematoma coagulates, a provisional matrix is structured for the healing process to progress [37] (Fig. 5c). Cartilage was used to biophysically model the soft callus repair phase, as structures composed of fibrin granulation tissue form, conducting the development of a collagenous fibrocartilaginous network surrounding the fracture biosurfaces [37]. Cartilaginous structures were obtained by extracting articular cartilage from femoral samples, which was followed by grounding and compression (Fig. 5d). As endochondral ossification of the cartilaginous callus takes place throughout the hard callus repair phase, culminating in the formation of a hard calcified callus of immature bone [37], trabecular bone was used to biophysically model the hard callus tissue. Initially, slices of cancellous bone lower than 5 mm thick were dissected; then, these were ground and compressed (Fig. 5e). Finally, the remodeling phase was biophysically modelled by intact bone, whose surface was thoroughly cleaned to remove any residual or fat tissues.

Concerning the experimental procedure, five tests were conducted for each healing phase to establish statistically significant capacitance changes. The experimental design followed the reverse progression of fracture healing: firstly, the remodeling phase (intact bone); secondly, the hard callus phase (cancellous structures); thirdly, the soft callus phase (cartilaginous structures); and, finally, the inflammatory phase (coagulated blood). This approach was adopted to prevent contamination of the bone surface due to the preceding phases, namely from the thinner callus to the larger hematoma. Throughout all healing phases, the samples were positioned 1 mm apart from each other to ensure consistent capacitive measurements (and according to simulation results), as well as to allow effective insertion of materials in the fracture. An additional test was conducted to evaluate the capacitive method to detect healing stages, by joining the two bone extremities to simulate more realistic fracture scenarios. For such purpose, a three-point bending test was performed to induce a fracture using the universal machine Shimadzu AGS-X-10 kN (Fig. 5f).

All experimental tests with biological tissues were performed at 22 °C and 50% humidity. While physiological conditions (37 °C) must be considered in future works, capacitance patterns are unlikely to be significantly different compared to the ones obtained under physiological conditions, as the sensor working principle is based on detecting capacitive variations, rather than absolute capacitance values.

Data normalization

The normalization process was necessary to take into account the magnitude differences found in capacitive

variations between simulation and experimental results, which arise mainly due to computational modelling approach based on simplified bone structures. The same normalization was performed to computational and experimental data, using the normalized capacitance values C_{norm} defined as

$$C_{norm} = \frac{C_i - C_{min}}{C_{max} - C_{min}}, \quad (8)$$

where C_i is the measured capacitance for a given region and stage, C_{min} is the minimum observed capacitance, and C_{max} is the maximum capacitance. This normalization ensures that all capacitance values are scaled between 0 and 1, allowing consistent comparisons across different conditions.

Similar capacitive variation patterns are expected for different sensor-fracture distance, even though different capacitance reactance magnitudes may occur. Indeed, each surgical procedure may result in different sensor-fracture distances, but such distances are usually not significantly different among surgeries, as similar medical protocols are followed to ensure plate-bone fixation. Throughout bone healing, no significant sensor-fracture distances are expected, even when stresses occur as the callus progresses.

Results

Mechanical tests

The commercial plate exhibited a stiffness of 874 N/mm, while a stiffness of 794 N/mm was measured for the new bioelectronic prototype (Fig. 6). Therefore, a prototype stiffness of 90.8% was obtained in comparison with the one provided by the commercial implant, exceeding the established target of 85% for a superior mechanical performance.

Capacitive sensing

Simulation results

A slight decrease (0.9%) in the peak capacitance was observed as the fracture size was decreased from 1 mm to 0.25 mm (Fig. 7). Similar capacitive variation patterns were obtained for different healing phases, including the inflammatory, soft callus, and hard callus stages. Notably, significant increases in capacitance were observed as the fractured region was approached with the most significant changes occurring during the inflammatory phase. Although the capacitance differences between the repair and remodeling phases were of lower magnitudes, they were still measurable, indicating distinguished dielectric bone properties, as the healing progresses. Results also highlight peak capacitance decreases as the healing progresses from the soft to the hard callus phase, mainly due to the reduced dielectric variations (and related electrical

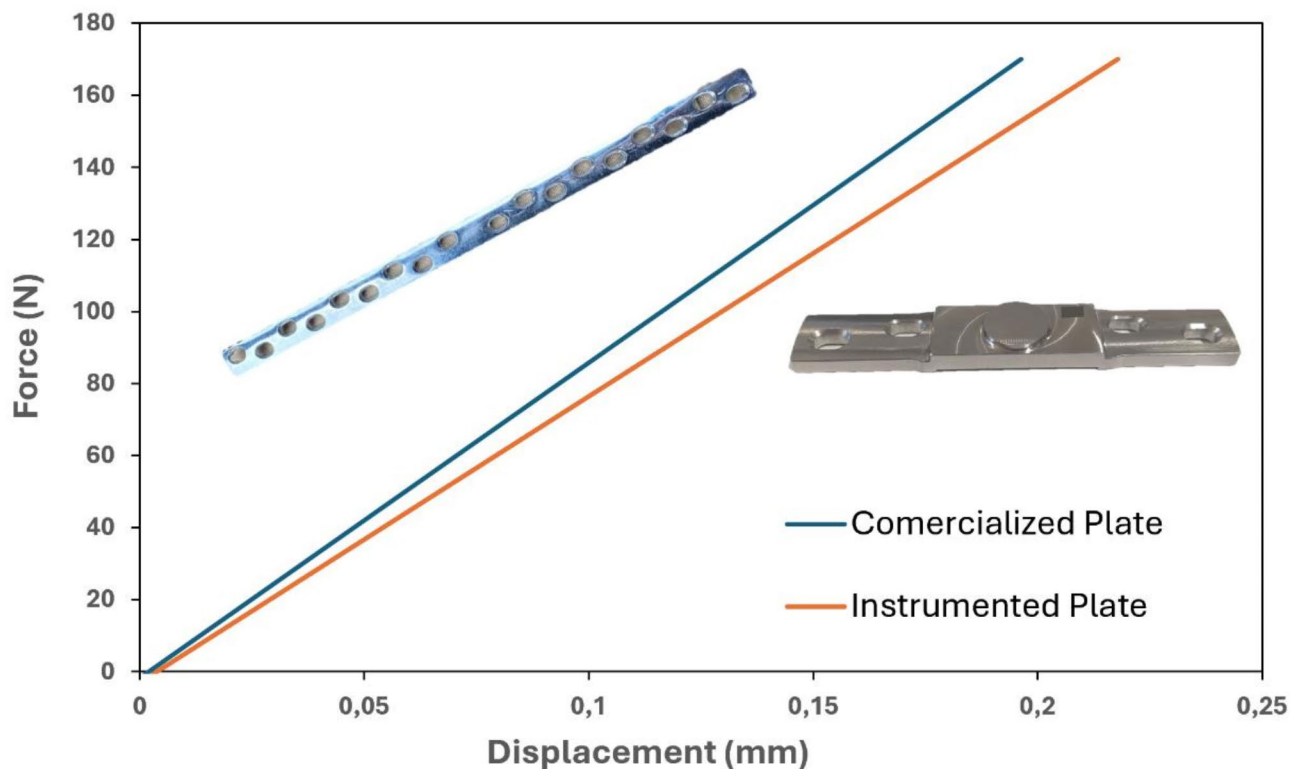


Fig. 6 Experimental results of the three-point bending test: comparison between new instrumented and commercialized plates

responsiveness) in the maturing tissue. Indeed, capacitances of 292.15 fF, 291.95 fF and 291.85 fF for 1 mm, 0.5 mm and 0.25 fractures, respectively, are predicted for the soft callus phase, while 290.69 fF, 290.69 fF and 290.52 fF for 1 mm, 0.5 mm and 0.25 fractures were found for the hard callus phase, corresponding to capacitance variations of 0.5%, 0.43%, and 0.46%. Furthermore, the steepest capacitance variations (8.67 fF for 1 mm fracture, 8.44 fF for 0.5 mm fracture, 7.64 fF for 0.25 mm fracture) are expected to occur in the inflammatory phase and the soft callus phase. When the healing process reaches the remodeling phase, non-significant capacitance variations occurred, as expected within healed bone tissues. These findings provide strong evidence that healing stage significantly influences the magnitude of capacitive changes, while non-relevant impacts are predicted for the fracture thickness. The latter finding supports the universality of our monitoring method based on electric capacitive variations, due to which only fracture scenarios with the 1 mm thickness were experimentally tested.

Experimental results

Similar capacitive variation patterns were found between experimental simulation findings. On the one hand, similar increases in capacitance were detected from intact bone regions toward the fractured regions; on the other hand, capacitance gradually decreased as the fracture

healing progressed from the inflammatory phase to the remodeling phase.

The experimental results revealed significant capacitive variations throughout the different stages of fracture healing, with the most pronounced increases occurring during the inflammatory phase, followed by gradual decreases as the healing process approaches the remodeling phase. The average capacitance increased by approximately 41.5% in the inflammatory phase from the intact regions to the fractured region, with peak capacitance values ranging from 1.23 pF to 1.74 pF (Fig. 8a). In the soft callus phase, the observed average capacitance change was around 11.3%, with peak values between 1.38 pF and 1.54 pF (Fig. 8b). A lower capacitance increase was detected in the hard callus phase, with an average change of approximately 8% (peak values ranging from 1.38 pF to 1.28 pF), as shown in Fig. 8c. Finally, the remodeling phase exhibited negligible capacitance variations, as peak values ranged between 1.1356 pF and 1.1345 pF (0.1% average variation) (Fig. 8d). The confidence intervals (CIs) revealed deviations reaching up to 0.7 pF and 0.53 for the 99% CI and 95% CI, respectively, in the hard callus stage. These larger confidence intervals most likely occurred due to parasitic capacitances influencing measuring. Lower deviations were found during the critical healing stages, namely 0.65 pF and 0.5 pF

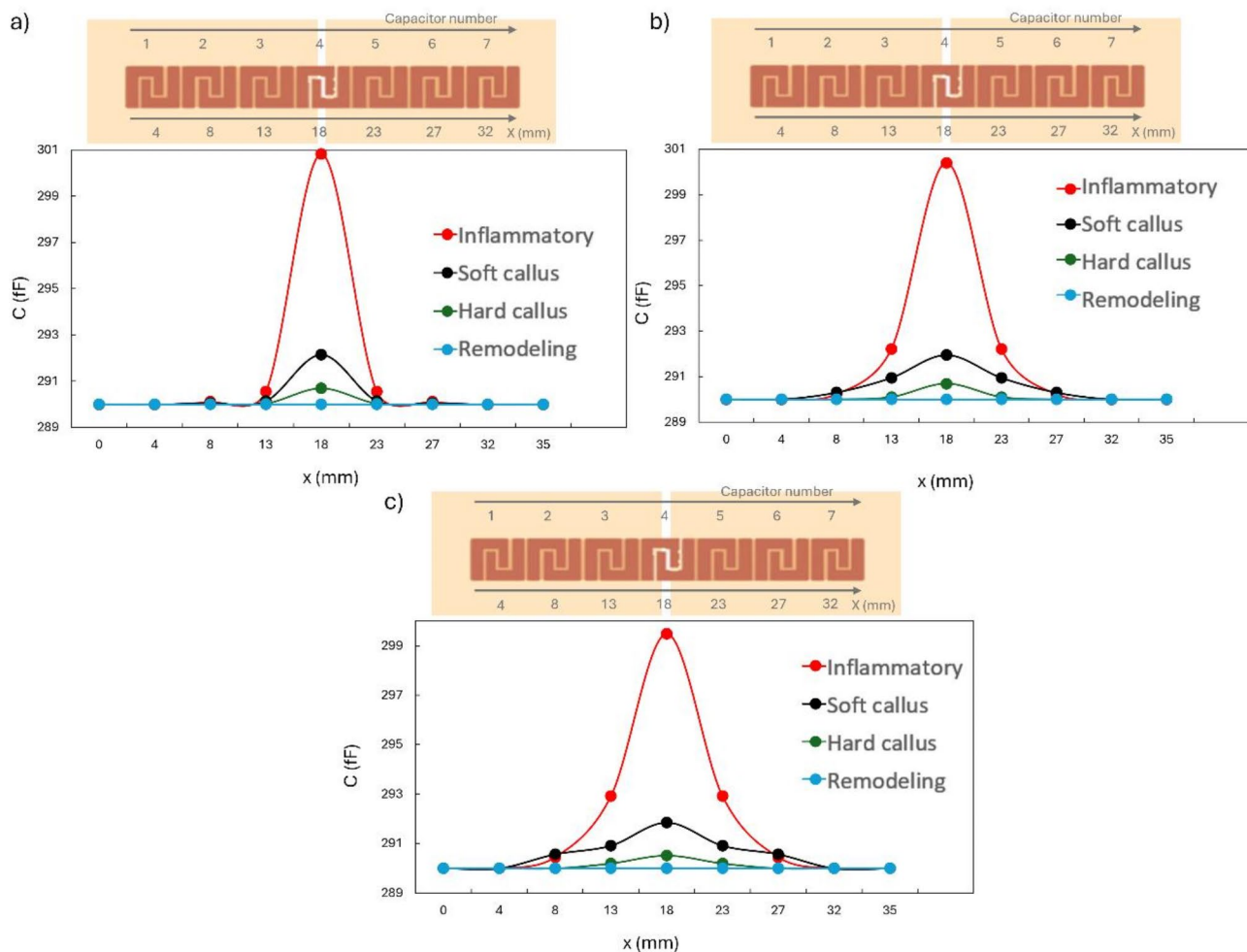


Fig. 7 Simulation results: **a)** for fractures with 1 mm; **b)** for fractures with 0.5 mm; **c)** and for fractures with 0.25 mm. A cubic spline data interpolation was used between different measures (data points)

for the soft callus stage, and 0.59 pF and 0.45 pF for the inflammatory stage.

Noticeable capacitance differences were also measured between the remodeling phase and the scenario characterized by bone extremities bonding (Fig. 8e): capacitance measures exhibited a variation of approximately 19%. This is a significant variation when compared with the near-stable capacitance observed during the remodeling phase, where 0.1% of capacitive variations were found. These are very relevant findings, as they highlight that even when the bone is fully joined, as usually occurs in realistic clinical settings, capacitive differences are still measurable, further supporting the sensing sensitivity to structural variations during bone healing.

Discussion

Figure 9 presents a comparative analysis of the computational and experimental results using normalized capacitance data for all bone regions and stages of bone healing. Both the experimental and computational curves exhibit

similar quasi-normal distribution patterns, with capacitance increases from the intact bone regions to the fractured region. Both simulation and experimental results also decrease capacitive variation patterns, reaching negligible variations when the healing is complete.

The major difference between computational and experimental apparatus was the different complexity of bone structures. Computational modelling was performed using simplified structures of bone tissue domains such that both reduce computation cost and predict the general capacitance variation patterns during bone healing. Apart from this issue, modelling-experimental differences result in negligible differences in capacitance measures. Included are the defined model domain sizes: cortical and trabecular bone sizes were computationally modelled with lower sizes in comparison to the experimental ones: nevertheless, negligible differences in capacitance variations are expected, because more distant bone extremities from the fracture region

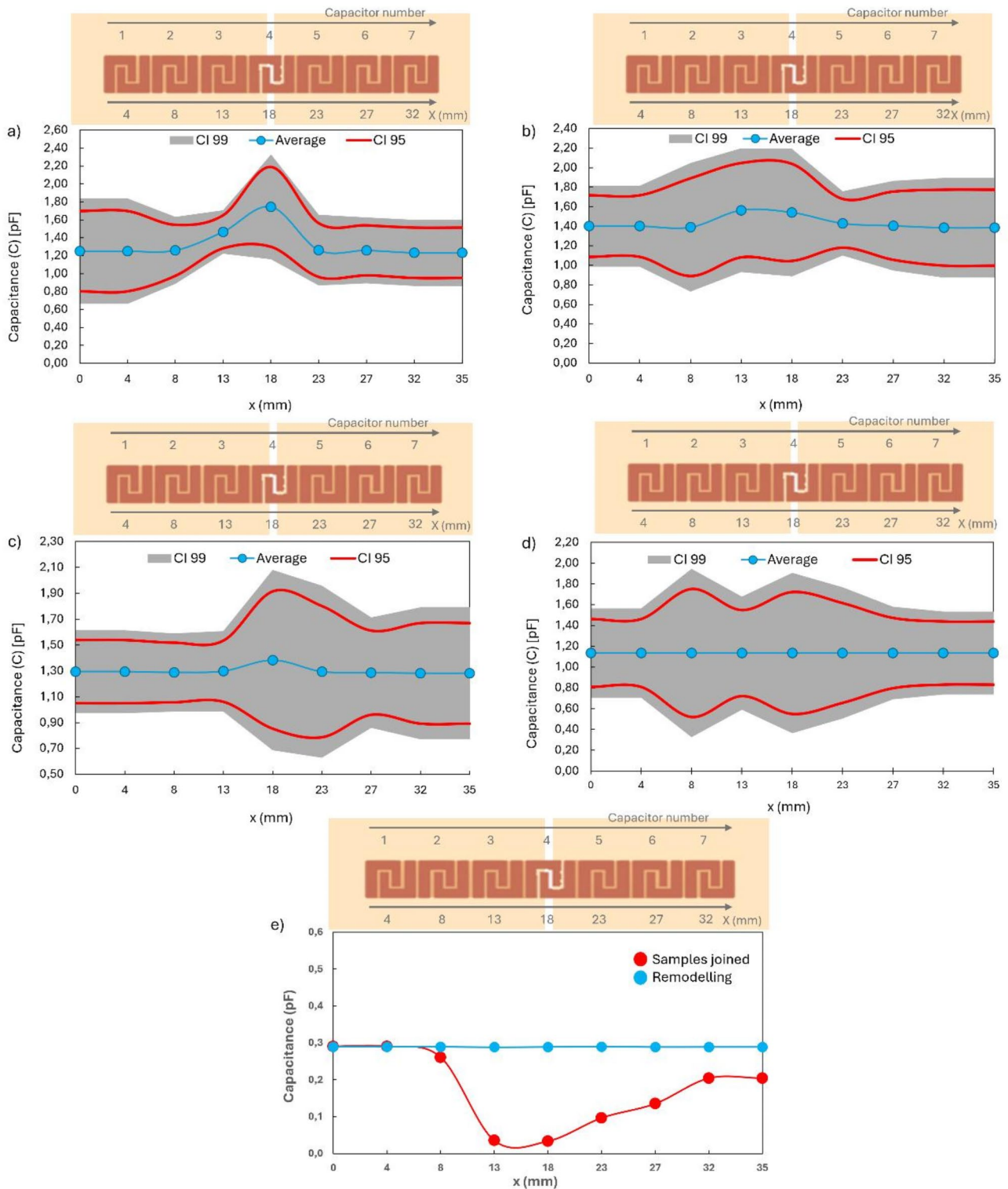


Fig. 8 Experimental results: each point expresses the average capacitance value from five independent measures for each fracture healing stage: **(a)** inflammatory phase; **(b)** repair phase (soft callus); **(c)** repair phase (hard callus); and **(d)** remodeling phase. The 99% CI and 95% CI were computed by standard deviation from the average capacitance found in the five bone samples; **(e)** Capacitance variation observed when the two bone extremities were joined compared to the remodeling phase. A cubic spline data interpolation was used between different measures (data points)

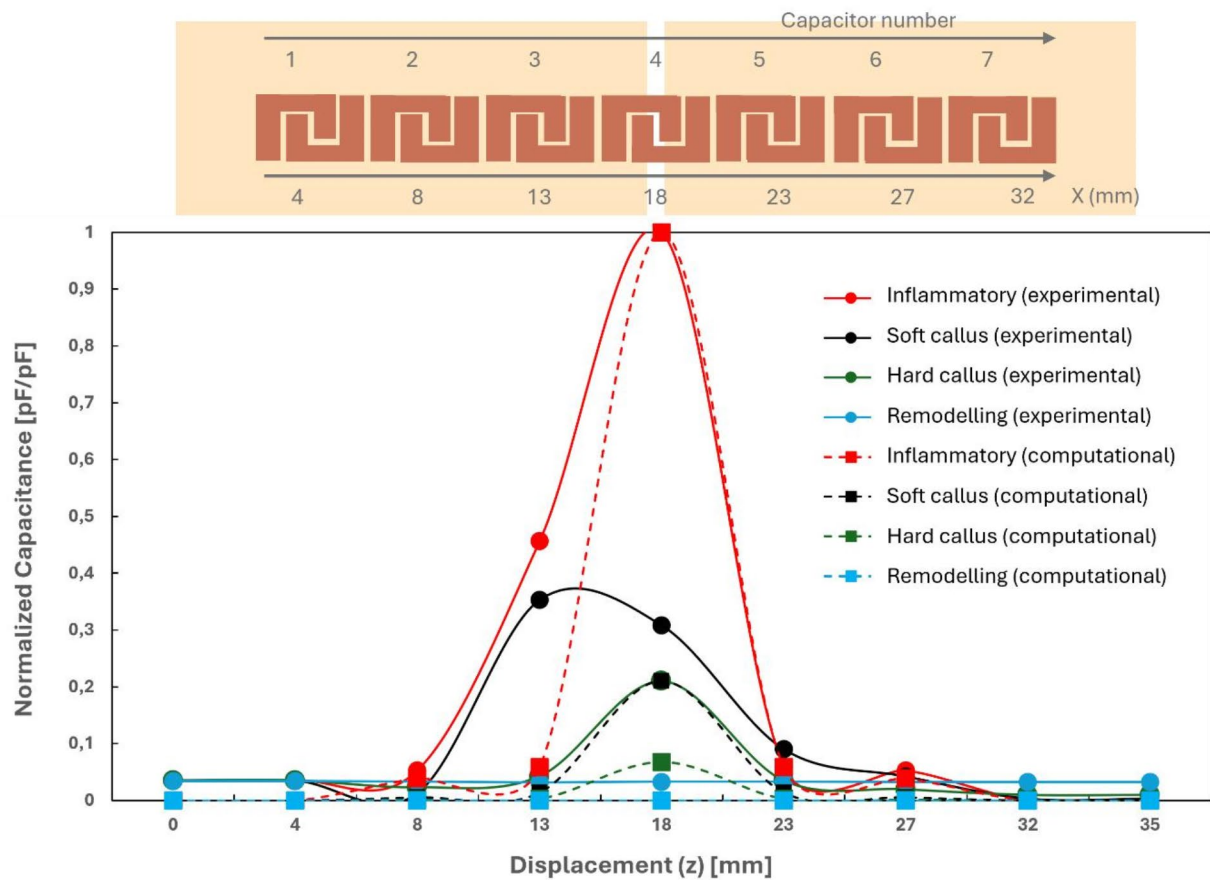


Fig. 9 Normalized capacitance variations from experimental and computational tests. A cubic spline data interpolation was used between different measures (data points)

Table 3 Percentual error analysis of each electrode pair across the four phases compared to experimental values

No. of electrode	1	2	3	4	5	6	7
Error in inflammatory phase (%)	4	1	40	0	0	1	0
Error in soft callus phase (%)	4	1	34	10	8	4	0
Error in hard callus phase (%)	4	2	4	14	3	2	1
Error in remodeling phase (%)	3	3	3	3	3	3	3

result in nonsignificant differences in electric field distributions in the vicinity of the fractured regions.

Table 3 highlights the percentual errors related to each electrode pair across the different healing stages. Most errors were found below 10%, even though a region near the fracture center (electrode 3) reached 40%. Correlations between the experimental and computational patterns of 92% for the inflammatory phase, 63% for the soft callus phase, and 99% for the hard callus phase, were obtained. These differences emerged most likely due to: (i) the irregular surface of the bone, while computational models assume a perfect cylindrical shape; (ii) highly inhomogeneous dielectric properties found in real bone morphology were not considered in computational models; (iii) the experimental fractures present some degree

of geometrical difference from the fracture model used in simulations; (iv) bone samples used to biophysically simulate the different healing phases are not homogeneous. Despite some differences between the computational and experimental results, it is clear that capacitive sensors are able to effectively detect dielectric changes in bone tissues throughout the healing process.

Current methods for monitoring bone fractures primarily rely on imaging techniques, which have significant limitations regarding detection objectivity, cost, and daily monitoring capabilities. Various alternative technologies have been proposed, including those based on mechanical vibration, electrical impedance, electromagnetic radiation, electric charge, and mechanical displacement. Additionally, some technological advances

have aimed to incorporate instrumented fixators into the monitoring process. However, despite extensive research efforts, none of these sensing technologies have proven to be effective for monitoring fracture healing. Indeed, they have not been designed to provide: (i) non-invasive operation; (ii) effective integration within fixation systems used in clinical practice, including their stand-alone sensing and data transfer; (iii) personalized monitoring of target tissues, including fractured and non-fractured ones; and (iv) daily basis fracture monitoring throughout all healing phases.

Our new concept of bioelectronic implant will most likely provide a suitable response to these challenges, by using an ultrasensitive detection method based on cosurface network-engineered capacitive sensors. Results from both experimental and numerical simulations hold potential to effectively detect the four distinct bone healing phases across target regions. Furthermore, simulation outcomes indicate that the developed computational models can predict capacitive variation patterns throughout all stages of fracture healing, achieving good experimental-simulation correlations (some exceeding 90%). Similar capacitive variation patterns are expected for different sensor-fracture distance, even though different capacitance reactance magnitudes may occur. Indeed, each surgical procedure may result in different sensor-fracture distances, but such distances are usually not significantly different among surgeries, as similar medical protocols are followed to ensure plate-bone fixation. Throughout bone healing, no significant sensor-fracture distances are expected even when stresses occur as the callus progresses. Additionally, to address patient idiosyncrasies, such as variations in capacitance baselines across patients, all data must be normalized to a common baseline. This will ensure that capacitance variations, which are the key to differentiating healing stages, remain consistent and comparable between different patients, enabling accurate and reliable detection of the bone healing process.

Our bioelectronic prototype was developed with mechanical characteristics similar to those used in current clinical practice, and it was engineered to incorporate a sensing system for measuring the healing states, as well as to facilitate data communication with extracorporeal systems. Importantly, this new bioelectronic plate does not interfere with the surgical procedures.

Regarding the sensing system, a new biomedical circuit was designed to connect and analyze multiple capacitive sensors, allowing remote communication and personalized patient monitoring. By creating a database, physicians can access monitoring data related to bone healing through a network connection to extracorporeal databases. When a delayed healing or non-union is detected, early intervention becomes possible through

various treatment types, including pharmacological and/or biophysical stimulation-based treatments. The administration of pharmacological therapies, using e.g. calcitonin, may result in improving bone consolidation as soon as healing conditions are detected [38]. Furthermore, the Jintiang capsule has been suggested as a potential promoter for osteoporotic fracture healing, by enhancing bone microstructure in aged rats [39]. The delivery of biophysical stimuli, such as Intermittent Pneumatic Compression (IPC), can also complement the sensing ability of bioelectronic implants by improving vascularization and tissue repair, contributing to a faster recovery [40]. Additionally, as the use of low-intensity pulsed ultrasound can promote osteoinduction [41], bone strength can be enhanced by monitoring data provided by sensing implants. Besides, bioelectronic implants comprising capacitive interdigitated structures can also be used to deliver targeted bioelectrical stimuli to the fractured regions, such that both osteoinduction and osteoconduction can be enhanced [22, 28]. By integrating these synergetic sensing-therapeutic approaches, comprehensive strategies for improving fracture management can be clinically approved by taking the opportunities provided by bioelectronic monitoring.

Conclusions

This work provides the design and implementation of an innovative bioelectronic osteosynthesis plate to monitor the bone-implant interface, such that the progression of bone fractures stages can be effectively detected. It was minimally customized from a fixation device used in clinical practice to allow easier clinical translation, and includes a biomedical circuit composed by a network-architected capacitive interdigitated system, a Bluetooth module, an analog-to-digital converter, a multiplexer, a microcontroller, and a miniaturized battery. Our research demonstrated that our bioelectronic implant is able: (i) to detect the four distinct bone healing stages, with capacitance decreases throughout the healing process; and (ii) to monitor the callus formation across multiple target regions.

Despite the promising results of our bioelectronic osteosynthesis plate additional research challenges must be addressed:

- Design, manufacture and test of a chip-size biomedical circuit with very high spatial resolution (at the micro-scale), such its container can be miniaturized.
- Investigate the performance of the bioelectronic implant under other types of fractures, including oblique and comminuted (fragmented) fractures. Additional analyses of other fracture scenarios are mandatory to support the use of this technology

in clinical practice, as generalized results will be obtained.

- Improve the powering system by introducing additional micro-size batteries to enable the sleep mode of the biomedical circuit throughout the fracture healing process. Alternatively, external power solutions, such as electromagnetic induction, can provide simultaneous charging and communication, using AM/FM modulation to facilitate energy transfer and data exchange without disrupting the device's functionality.
- Develop computational models with more realistic bone structures, using e.g. micro-CT imaging to capture the structural complexity of fractures.
- Implementation of a superior detection capability by significantly reducing parasitic capacitive effects and increasing the sensitivity of capacitors. This will require optimizing the electrode surface area and finding the optimized space between electrodes, such that interference can be minimized, and measurement accuracy can be enhanced [42].
- Development of an actuation system capable of delivering electrical stimuli to the fracture region to accelerate and/or enhance fracture healing.
- Analyze the performance of bioelectronic implant under in vivo testing on animal models, both for personalized healing detection and biophysical stimulation. This will provide essential details about the performance in living biological environments, mainly related to idiosyncrasies of animal models and human-like scenarios, filling the gap for supporting clinical trials. For this, the first step involves sealing the entire implant, including the integrated circuit, within the prosthesis. A biocompatible polymer will be used to vulcanize the implant, ensuring a durable and safe interface with biological tissues. The vulcanization process not only insulates the circuit from corporal fluids but also maintains the mechanical stability of the implant during the healing process. Additional tests must be performed, including the assessment of the device's failure strength, biocompatibility, hermeticity of the exposed PCB, and sensing robustness under strain on the implant. Although the stiffness of the new plate reached more than the 85% targeted of commercial plates, further evaluation is needed to confirm its reliability under diverse stress conditions. These tests must comply with the ISO 9585 standard to ensure valid assessments of the mechanical performance of bioelectronic osteosynthesis plates.

Supplementary Information

The online version contains supplementary material available at <https://doi.org/10.1186/s13018-025-05534-4>.

Supplementary Material 1

Author contributions

D.P.: formal analysis, investigation, methodology, software, writing—original writing—review and editing; N.S.: formal analysis, investigation, methodology, software, writing—review and editing; A.C.: methodology, validation, writing—review and editing; M.P.S.d.S.: conceptualization, formal analysis, funding acquisition, methodology, project administration, resources, supervision, validation, writing—original writing—review and editing. All authors gave final approval for publication and agreed to be held accountable for the work performed therein.

Funding

This work was supported by the Portuguese Foundation for Science and Technology (PhD scholarship: 2024.01927.BDANA; project references: UIDB/00481/2020, DOI <https://doi.org/10.54499/UIDB/00481/2020>, <https://doi.org/10.54499/UIDB/00481/2020>; UIDP/00481/2020, DOI <https://doi.org/10.54499/UIDP/00481/2020>, <https://doi.org/10.54499/UIDP/00481/2020>).

Data availability

The data that support the findings of this study are available from the corresponding authors upon request.

Declarations

Ethics approval and consent to participate

Not applicable.

Consent for publication

Not applicable.

Competing interests

The authors declare no competing interests.

Received: 30 October 2024 / Accepted: 22 January 2025

Published online: 29 January 2025

References

1. Wu AM, et al. Global, regional, and national burden of bone fractures in 204 countries and territories, 1990–2019: a systematic analysis from the global burden of disease study 2019. *Lancet Health Long*. 2021;2(9):580–92.
2. Wildemann B, Ignatius A, Leung F, Taitsman LA, Smith RM, Pesántez R, Stoddart MJ, Richards RG, Jupiter JB. Non-union bone fractures. *Nat Rev Dis Primers*. 2021;7:57.
3. Nicholson JA, Yapp LZ, Keating JF, Simpson AH. Monitoring of fracture healing: update on current and future imaging modalities to predict union. *Injury*. 2021;52:29–34.
4. Bizzoca D, Vicenti G, Caiaffa V, Abate A, Carolis OD, Carrozzo M, Solarino G, Moretti B. Assessment of fracture healing in orthopaedic trauma. *Injury*. 2020;1383:30940–2.
5. Labus KM, Sutherland C, Notaros BM, Ilic MM, Chaus G, Keiser D, Puttlitz CM. Direct electromagnetic coupling for non-invasive measurements of stability in simulated fracture healing. *J Orthop Res*. 2019;37:1164–71.
6. Mattei L, Fonzo MD, Marchetti S, Puccio FD. A quantitative and noninvasive vibrational method to assess bone fracture healing: a clinical case study. *Int Biomech*. 2021;8:1–13.
7. Lin MC, Hu D, Marmor M, Herfat ST, Bahney CS, Maharbiz MM. Smart bone plates can monitor fracture healing. *Sci Rep*. 2019;9:2122.
8. Ernst M, Baumgartner H, Dobeles S, Hontzsch D, Pohlemann T, Windolf M. Clinical feasibility of fracture healing assessment through continuous monitoring of implant load. *J Biomech*. 2021;116:110188.
9. Symeonidis S, Whittow WG, Zecca M, Panagamuwa C. Bone fracture monitoring using implanted antennas in the radius, tibia and phalange heterogeneous bone phantoms. *Biomed Phys Eng Express*. 2018;4(4):045006.
10. Chiu W, Ong W, Russ M, Tran T, Fitzgerald M. Effects of mass loading on the viability of assessing the state of healing of a fixated fractured long bone. *J Rehabil Assist Technol Eng*. 2019;6.

11. Windolf M, Varjas V, Gehweiler D, Schwyn R, Arens D, Constant C, Zeiter S, Richards RG, Ernst M. Continuous implant load monitoring to assess bone healing status—evidence from animal testing. *Medicina*. 2022;58(7):858.
12. Kienast B, Kowald B, Seide K, Aljudaibi M, Faschingbauer M, Juergens C, Gille J. An electronically instrumented internal fixator for the assessment of bone healing. *Bone Jt Res*. 2016;5(5):191–7.
13. Wolynski JG, Labus KM, Easley JT, Notaros BM, Ilic MM, Puttlitz CM, McGilvray KC. Diagnostic prediction of ovine fracture healing outcomes via a novel multi-location direct electromagnetic coupling antenna. *Ann Transl Med*. 2021;9:1–20.
14. Borchani W, Aono K, Lajnef N, Chakrabarty S. Monitoring of postoperative bone healing using smart trauma-fixation device with integrated self-powered piezo-floating-gate sensors. *IEEE Trans Biomed Eng*. 2016;63(6):1463–72.
15. Pelham H, Benza D, Millhouse PW, Carrington N, Arifuzzaman M, Behrend CJ, Anker JN, DesJardins JD. Implantable strain sensor to monitor fracture healing with standard radiography. *Sci Rep*. 2017;7:1489.
16. Chiu WK, Vien BS, Russ M, Fitzgerald M. Healing assessment of fractured femur treated with an intramedullary nail. *Struct Health Monit*. 2021;2:782–90.
17. Wolynski JG, Sutherland CJ, Demir HV, Unal E, Alipour A, Puttlitz CM, McGilvray KC. Utilizing multiple biomems sensors to monitor orthopaedic strain and predict bone fracture healing. *J Orthop Res*. 2019;3:1873–80.
18. Ji X, Zhao D, Xin Z, Feng H, Huang Z. The predictive value of stress-induced hyperglycemia parameters for delayed healing after tibial fracture post-surgery. *J Orthop Surg Res*. 2024;19(1):666.
19. Li Y, Sun Y, Ma K, Wang S, Wang Z, Huang L. Functional mechanism and clinical implications of LINC00339 in delayed fracture healing. *J Orthop Surg Res*. 2024;19(1):511.
20. Zhang Z, Wang L, Zhang F, Jing S, Cen M. Functional mechanism and clinical implications of mir-1271-5p in pilon fracture healing processes. *J Orthop Surg Res*. 2024;19(1):782.
21. Wu X, Shen T, Ji W, Huang M, Sima J, Li J, Song H, Xiong W, Cen M. IncRNA CASC11 regulates the progress of delayed fracture healing via sponging miR-150-3p. *J Orthop Surg Res*. 2024;19(1):757.
22. Sousa BM, Correia CR, Ferreira JA, Mano JF, Furlani EP, Soares Dos Santos MP, Vieira SI. Capacitive interdigitated system of high osteoinductive/conductive performance for personalized acting-sensing implants. *Npj Regen Med*. 2021;6:1–14.
23. Silva NM, Santos PM, Ferreira JAF, Santos MPS, Ramos A, Simões JA, Reis M, Morais R. Power management architecture for smart hip prostheses comprising multiple energy harvesting systems. *Sens Actuator Phys*. 2013;202:183–92.
24. Soares Dos Santos MPS, et al. Towards an effective sensing technology to monitor micro-scale interface loosening of bioelectronic implants. *Sci Rep*. 2021;11:3449.
25. Sorriento A, Chiurazzi M, Fabbri L, Scaglione M, Dario P, Ciuti G. A novel capacitive measurement device for longitudinal monitoring of bone fracture healing. *Sensors*. 2021;21(19):6694.
26. Rolo P, Vidal JV, Kholkin AL, Santos MPS. Self-adaptive rotational electromagnetic energy generation as an alternative to triboelectric and piezoelectric transductions. *Comms Eng*. 2024;3(1):105.
27. Conceição C, Completo A, Soares Dos Santos MP. Ultrasensitive capacitive sensing system for smart medical devices with ability to monitor fracture healing stages. *J R Soc Interface*. 2023;20(199):20220818.
28. Pires DG, Silva NM, Sousa BM, Marques JL, Ramos A, Ferreira JAF, Morais R, Vieira SI, Santos MPS. A millimetre-scale capacitive biosensing and biophysical stimulation system for emerging bioelectronic bone implants. *J R Soc Interface*. 2024;21(218):20240279.
29. Kraus JD, Fleisch DA. *Electromagnetics with applications*. 5th ed. Boston: WCB/McGraw-Hill, Boston;; 1999.
30. Morais R, Frias CM, Silva NM, Azevedo JLF, Seródio CA, Silva PM, Ferreira JAF, Simões JAO, Reis MC. An activation circuit for battery-powered biomedical implantable systems. *Sens Actuator Phys*. 2009;156(1):229–36.
31. Asri RIM, Harun WSW, Samykano M, Lah NAC, Ghani SAC, Tarlochan F, Raza MR. Corrosion and surface modification on biocompatible metals: a review. *Mater Sci Eng C*. 2017;77:1261–74.
32. Li J, Qin L, Yang K, Ma Z, Wang Y, Cheng L, Zhao D. Materials evolution of bone plates for internal fixation of bone fractures: a review. *J Mater Sci Technol*. 2020;36:190–208.
33. Yang J-C, Lin K-P, Wei H-W, Chen W-C, Chiang C-C, Chang M-C, Tsai C-L, Lin K-J. Importance of a moderate plate-to-bone distance for the functioning of the far cortical locking system. *Med Eng Phys*. 2018;5:48–53.
34. Feng Y-J, Lin K-P, Tsai C-L, Wei H-W. Influence of gap distance between bone and plate on structural stiffness and parallel interfragmental movement in far-cortical locking technique—a biomechanical study. *Comput Methods Biomech Biomed Engin*. 2021;2:1206–11.
35. Soares Dos Santos MP, et al. New Cosurface capacitive stimulators for the development of active osseointegrative implantable devices. *Sci Rep*. 2016;6:30231.
36. Gabriel C, Gabriel S, Corthout E. The dielectric properties of biological tissues: I. literature survey. *Phys Med Biol*. 1996;41:2231–49.
37. Sheen JR, Garla VV. *Fracture Healing Overview*. Treasure Island: StatPearls Publishing; 2022.
38. Migliorini F, Cocconi F, Vecchio G, Schaefer L, Koettnitz J, Maffulli N. Pharmacological agents for bone fracture healing: talking points from recent clinical trials. *Expert Opin Investig Drugs*. 2023;32(9):855–65.
39. Liu J, Liu T-T, Zhang H-C, Li C, Wei W, Chao A-J. Effects of Jintiang on the healing of osteoporotic fractures in aged rats. *J Orthop Surg Res*. 2024;19(1):828.
40. Khanna A, Gougoulas N, Maffulli N. Intermittent pneumatic compression in fracture and soft-tissue injuries healing. *Br Med Bull*. 2008;88(1):147–56.
41. Albornoz P, Khanna A, Longo UG, Forriol F, Maffulli N. The evidence of low-intensity pulsed ultrasound for in vitro, animal and human fracture healing. *Br Med Bull*. 2011;100:39–57.
42. Wei L, Boeuf F, Skotnicki T, Philip Wong H. Parasitic capacitances: Analytical models and Impact on Circuit-Level performance. *IEEE Trans Electron Devices*. 2011;58(5):1361–70.

Publisher's note

Springer Nature remains neutral with regard to jurisdictional claims in published maps and institutional affiliations.